Measurement of Doppler Broadening in Vapor-limited Iodine Vapor Cells

T. Ayers, S. Cart, M. Dahal, E. Hagler, N. Hupp, D. Minich, R. Stipanovich, V. Tobar Correa, C. Vernon and M. Crescimanno*

Department of Physics and Astronomy,

Youngstown State University, Youngstown, OH, 44555

(Dated: November 14, 2026)

Abstract

Although one of the very first things students learn about gas-phase optical absorption spectra is that thermal motion relative to the light source contributes to the measured absorption linewidth (Doppler broadening), there is an acute lack of actionable literature on simple quantitative measurements of this effect for the undergraduate physics laboratory. Primarily this is due to large, obscuring resonant and non-resonant collisional effects, optical pumping effects, spectra fine structure, optical depth effects and lineshape distortion from a host of other processes that can contribute to the observed temperature dependence of an optical resonance's linewidth. Here we describe a straightforward, low-cost laboratory for isolating this universal kinetic theory contribution to the spectral linewidth broadening using small, easy to make vapor-limited iodine vacuum cells and inexpensive low-power 520nm semiconductor diode lasers. Using nothing more sophisticated than gaussian curve fitting, students measure a Doppler broadening of the full Gaussian width of absorption features near 520nm. An average indicating the universality of these mutually consistent measurements (across a dozen different spectral features) results in 19.7±3 $\sqrt{T}$ MHz, close to and consistent with the kinetic theory expectation of 22.05 $\sqrt{T}$ MHz.

I. INTRODUCTION:

It has become increasingly common for undergraduate physics students to learn the basics of laser spectroscopy as part of their upper division laboratory. Whether these explore the fine- or hyperfine structure of the absorption spectra of alkalis, or measure an isotope shift or involve a laboratory in molecular spectra, they all typically employ a tunable solid state diode laser, a glass sample cell and a Fabry-Perot cavity used as a frequency "ruler". Invariably these laboratory experiments display what instructors typically call Doppler broadened resonance lineshapes. While that moniker is intuitive, it belies the deeper reality that none of the line widths that students actually measure are easily relatable to the Doppler effect! The reason for that is the rich variety of contributing physical effects to the spectral linewidth including resonant and non-resonant collisional effects, optical pumping effects, level structure near degeneracy, optical depth (propagation) effects and instrumental lineshape distortions among many other processes.[1] Systematically removing these complexities reveals the underlying Doppler broadening contribution to the absorption feature's spectral width, universal to every absorption feature. Doing so results in a pedagogically simple experiment and analysis, ideal for the undergraduate advanced laboratory.

Very sophisticated approaches to understand atomic and molecular lineshape at ordinary temperatures are at the heart of "Doppler Broadening Thermometry" (DBT) metrological approaches and their precision application to a determination of Boltzmann's constant.[2–4] These references used ammonia and carbon dioxide, but the Doppler broadening in molecular iodine has also extensively studied[5], and the iodine dimer has been found to be a useful target for sophisticated precision metrological work that relies on deeply understanding lineshape.[6,7] The alkalis have also recently attracted renewed attention in DBT-related precision lineshape work.[8–13] Even contributions to lineshape distortions from dispersion across a single resonance line and higher order relativistic effects have attracted theoretical attention.[14] For a concise history of the development of these methods the reader may find the synopsis in[15] useful whereas a more current review can be found in[16,17].

Here we describe an inexpensive and easy-to-implement laboratory that directly quantitatively measures the universal (level-independent) Doppler contribution to the resonance linewidth using laboratory equipment available to an undergraduate advanced laboratory. This experiment is relevant to either a modern or a thermo-/statistical mechanics laboratory.

It uses only commercially available and inexpensive laser sources, cells and electronics. The most expensive part of this laboratory is a relatively low finesse, broadband Fabry-Perot cavity, though that can be substituted (by, for example, an Michelson interferometer) if preferred. An important goal of our approach was to forgo having students use proprietary fitting software, or black-box custom Voigt (or other) absorption feature fitting routines in favor fitting with a single Gaussian. Doing so reinforces what students learn in their modern physics course or statistical mechanics course, via the Gaussian velocity distribution associated with kinetic theory of an ideal gas. This protocol's educational value is as a laboratory experience that yields a measurement of the Doppler effect that is statistically consistent with and routinely within 15% of the simple kinetic theory value.

The main simplifying step we adopted here is the creation and use of thin, vapor-limited (sometime called "depleted") iodine cells, an admittedly old idea.[18] Over the temperature range we employ these vapor cells the number density of volatilized resonant molecules remains constant; this serves to restrict temperature-dependent changes in the collisional contribution to the spectral linewidth. This is in contrast to undepleted and "cold finger" experimental methods (which we refer to as constant pressure cells, as for example in[19]).

We use cells with optical paths that are at most a few mm long, akin to the very thin cells used for a similar purpose in[20]. Using thin cells alleviates complicating propagation effects (such as radiation trapping and multiple scattering) while yet exploring a large temperature range. The typical commercially available 10cm long iodine vacuum cells (not depleted) are particularly troublesome in this regard as there are so many nearby resonances that contribute to the resonance's pedestals at 520nm that even minor absorption features that alone might not saturate at higher temperatures achieve large optical depth at relatively low temperatures, greatly limiting the temperature range over which to measure the Doppler broadening part. Of course, the fact that the typical vacuum Iodine spectroscopy cell is not depleted and has no useful cold finger means that there are large changes in the line contrast with temperature which tend to distort the determination of the linewidth, even far from large optical depths. We do note that long (10cm) depleted (though usually buffer gas filled) Iodine cells have found use in recent frequency standards.[21]

Since every warm atom/molecule absorption signature has a thermal Doppler profile, why choose Iodine? We chose to work with molecular Iodine for several key reasons. First, the plethora of resonance lines (as compared to the sparse ground state excitation spectra of the

commonly used alkalis) near the wavelengths of inexpensive, readily available laser sources coupled with the universal nature of the Doppler width for every resonance line means that virtually any 520nm laser diode will work for this lab. We find that typically, with just heating any of these diode, one typically has access to roughly 10 suitable I_2 absorption lines for this experiment. For the alkalis typically only about 1 in 4 diodes are suitable for the ground state transitions, and the tuning is a bit more exacting that used here with Iodine. Second, Iodine is chemically significantly more inert than the alkalis, which have a tendency to chemically react and diffuse into the glass container, a process that is exacerbated at high temperatures required for this experiment.[19] We have not been able to record any change in the optical behavior of our depleted Iodine cells in many thermal cycles. Third, making a depleted Iodine vacuum cell is technically much easier (see instructions below) than one with an alkali which may require a processing in a nitrogen purged hood to avoid oxidation of the alkali. Of note, all the cells used in this experiment were made by the student co-authors.

For completeness the supplemental material to this note contains a brief derivation of Maxwell's distribution but here for brevity we include just its use relevant to the laboratory. Since the non-relativistic energy E is proportional to the sum of the squares of the cartesian components of the velocity, the Maxwell-Boltzmann result factorizes, indicating that the probability that a molecule has velocity component v_x along the direction of the laser beam's propagation is

$$P(v_x) \sim e^{-\frac{\beta}{2}mv_x^2} \sim e^{-\frac{\beta m\lambda^2}{2}(\Delta f)^2} \tag{1}$$

(here λ is the wavelength of the laser light that is detuned a frequency Δf from the center frequency of a narrow molecular resonance) where we have used the Doppler relation $\Delta f = (1 - v_x/c)f$. Thus naively one expects the absorption of laser light as a function of detuning from a spectrally isolated, narrow resonance to be Gaussian and directly mirror the shape and size of the underlying one-dimensional slice of the Maxwell-Boltzmann distribution.

In a more general setting, this gaussian width must be convolved with all the nearly resonant line(s) that contribute to an absorption feature. This may be approximated as a convolution of gaussians, meaning that the individual widths add in quadrature. We expect then an isolated absorption feature's total (gaussian) width, Γ to behave approximately as

$$\Gamma(T)^2 = \Gamma(0)^2 + \frac{4k_B}{m\lambda^2}T \tag{2}$$

so for the Iodine dimer we expect a slope with temperature of the square of the full Gaussian

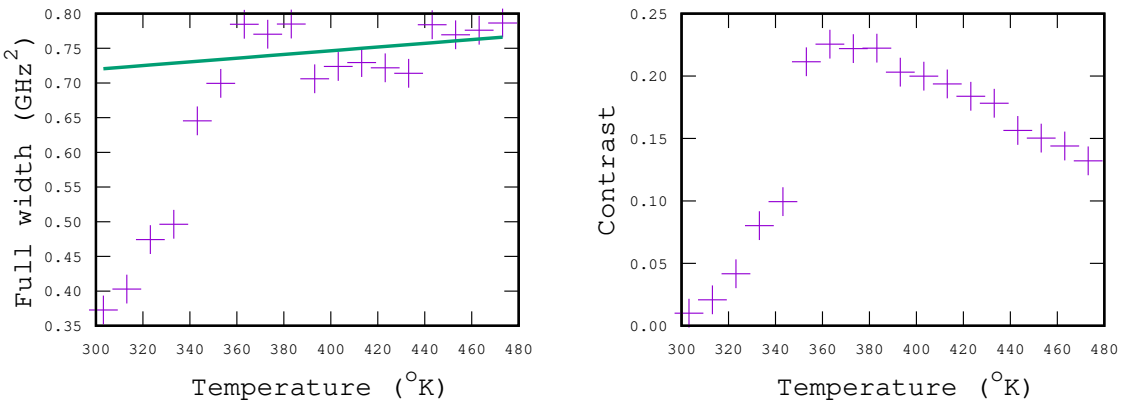

FIG. 1. (a) Resonance growth width in a typical narrow but undepleted Iodine vacuum and,(b) the associated line contrast as functions of the temperature. The large changes in the contrast are in part due to the significant changes in the Iodine vapor density (pressure) with temperature. These contrast changes have a profound effect on the growth of the measured feature spectral width. Even restricting attention to just the temperature region in which the contrast is changing more slowly (after 350°K here, line is linear best fit) the slope of the width growth is 16$\pm$8 $\sqrt{T}$ MHz.

width to be 486 MHz^2 ^{o}K which we report in terms of the expected square root growth of the full linewidth, 22.05 $\sqrt{(T)}$ MHz.

To help the reader understand the practical nature of the problem, Fig.1 summarizes the width growth and contrast change of a typical absorption line as one increases the temperature on a miniature (1.5mm thick) undepleted vacuum iodine cell. These are cells which during manufacturing have Iodine in excess of the near room temperature equilibrium vapor pressure. This means that there is a substantial solid phase portion in the cell that, as one increases the temperature, continues to sublime. This increases the optical density leading greater contrast of the absorption line (Fig.1b before $\sim$350K for that cell). As one increases the temperature further the absorption pedestal around the resonance line darkens more quickly than the optical line (which at large optical depths saturates), leading to an apparent decrease in line contrast (Fig.1b after $\sim$350K).

These profound changes in the vapor density lead also to large changes in the fitted gaussian width Fig.1a. Here plotted as the square of the gaussian width, thermal Doppler broadening indicates that these data should be linear in the temperature. A linear fit for even a portion of these data generally leads to a width growth with temperature that is

significantly smaller than the Doppler expectation. These effects are particularly acute at 520nm in the typical commercially available vacuum iodine cell, which is 10cm long and undepleted. The long optical path in those cells significantly limits the temperature range one can study for all but the most muted absorption lines (before the Voigt profile fitting is necessary). We have found at this wavelength that for even a minor absorption line, the combined effect of the lineshape distortions from saturation and pedestal growth still limit the useful temperature range in these long cells to below 345°K. Worse, the absorption lines of minor lines typically appear to become spectrally more narrow with increasing temperature. This is from the unavoidable differential growth between the pedestal and the optical depth on resonance. A practical student laboratory using long, undepleted vapor cells that removes these confounding factors from the width data so as to quantitatively resolve the Doppler component is beyond the scope of this paper.

Consider now a depleted Iodine vacuum cell. The vapor pressure of Iodine is well modelled with the Antoine equation (available publicly at NIST Chemistry WebBook[22]) as

$$log_{10}(P) = A - \frac{B}{T+C} \qquad \text{for} I_2 \qquad A = 3.364, B = 1039, C = -146.6 \tag{3}$$

where in the above expression the pressure P is in bar and the temperature T is in ^{o}K. For a typical depleted cell made a bit above room temperature then the pressure is nearly a millibar, indicating that the mean free path is about 100 μm. Since a typical average speed of the Iodine dimer at these temperatures is about 100 m/s, the collision rate is atmost in the few MHz range throughout, which is much smaller than both the Doppler effect and the typical transition linewidths. At these densities an Iodine molecule spends on average only about one hundred-thousandth of its time close to another Iodine molecule, so that it is isolated the vast majority its time interacting with the radiation field. Subsequently comparing our cell's absorption features with that of a commercial cell (as well as the pressure gauge reading during the cell construction) gives us confidence that any residual (non-Iodine) gas was also below this pressure.

II. THE EXPERIMENT:

Iodine is ideal spectroscopic target in part for its rich set of bright resonances across the range of the available spectrally narrow, inexpensive laser diode sources at 520nm. Since

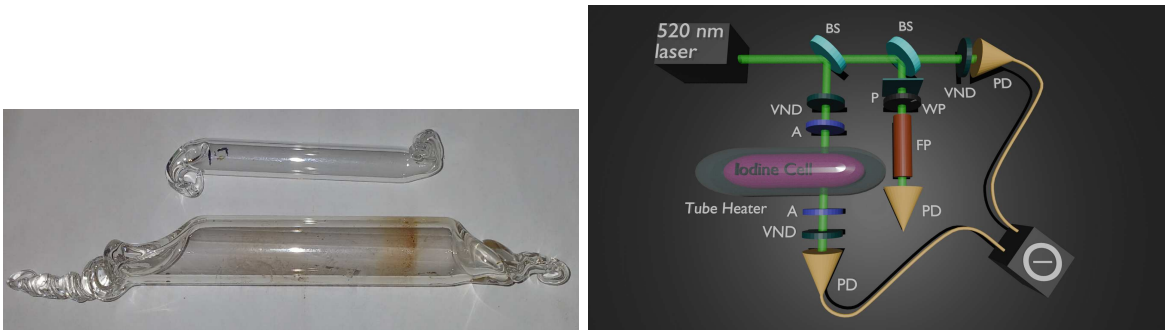

FIG. 2. (a) Typical depleted Iodine vacuum cells, made as described in the text. (b) Schematic of the experiment. BS beam splitter, VND variable neutral density plates, P polarizer, WP quarter wave plate, PD photodiodes, A apertures.

the Doppler process we are measuring is universal to all the lines, we have not endeavored to actually label our particular transitions against the nomenclature of the Iodine atlas[23]. We instead focus our attention on any spectroscopically well isolated and symmetric absorption features in the mode-hop free, temperature tuned range of the diode lasers.

Perhaps the least familiar part of implementing this laboratory is making the thin, depleted vacuum Iodine spectroscopy cells (Figure 2a). One end of a section ($\sim$ 30 cm long, ID 2.5mm or 1mm) of straight borosilicate tubing was heated and twisted into a sealed end. The tube was then cooled and loaded with a minute grain of solid iodine resting on the sealed end. That end was then heated gently to vaporize the iodine grain while the tube was continuously rotated by hand to distribute the condensing iodine vapor over the inner glass surface.

In anticipation of a vacuum sealoff, a section about midway of the tube was then heated and twisted to neck the tube down to near seal. After allowing the whole tube to cool the far open end was attached to the foreline of a mechanical vacuum pump using a mechanically compressed seal. The pump was then turned on briefly to reach its lowest attainable pressure and then turned off, the foreline valve maintaining the established vacuum.

With some height between the flame and the assembly, a temperature gradient was applied along the length of the tube, with the hottest end being somewhat near the open end connected to the foreline, and the far (already near seal + sealed) end kept cooler, encouraging redistribution of residual iodine toward the cooler arm at this reduced vapor pressure. That section closest to the foreline is then heated and twisted to a seal. Finally

then the partially twisted section in the middle at the near seal was heated, softened, twisted closed and separated from the sealed section retaining the iodine. What remains is then an evacuated, iodine-depleted cell typically of about 6 to 8cm in length.

The presence of residual iodine in an evacuated, iodine-depleted cell was verified by two methods. The cell was heated and visually inspected against a white backdrop for the characteristic coloration of iodine vapor. A sufficiently iodine-depleted cell typically visually demonstrated very little to none of the expected purple iodine vapor. The presence of Iodine was further verified spectroscopically by sweeping the laser frequency (using a current ramp) over resonances while comparing the absorption of its light to absorption in a commercial, 10 cm long, room temperature vacuum Iodine reference cell. That is, similar absorption features in both cells confirm the presence of residual iodine in the depleted cell. Finally a candidate cell was determined to be depleted if the contrast varied by less than 15% over a range of elevated temperatures.

The optical layout of the experiment itself is rather conventional for transmission spectroscopy(2b). A 520nm laser diode (OSRAM PLT5 520DB_P or PLT5 520EB_Q) is collimated and incident upon a 50/50 plate beam splitter (Thorlabs BS037) which breaks the beam into a "reference" and a "signal" beam. Part of the "reference" beam is fed to a photodiode behind an iris and a variable neutral density filter, the rest of the reference beam is sent into a commercial confocal broadband Fabry-Perot cavity (Thorlabs SA200-5B) with a finesse of ~ 200 and a free spectral range 1510MHz. The "signal" beam travels through the Iodine cell on its way to a second photodiode. The photodiodes (OSRAM BPW 34) are matched and are each attached to matching transimpedance amplifiers (with 1 MΩ feedback resistors) based on separate TL062 chips each co-located with its photodiode. Both amplifiers are driven by the same $\pm$9V split power supply that is has no common ground ("cabinet ground") with the rest of the experiment's electronics. Instead, the output of one of the photodiode amplifiers is tied to the cabinet ground, the other's output being the signal fed to oscilloscope, thus facilitating a balanced detection scheme even for a scope without true differential inputs. We also use two variable neutral density filters to facilitate the balancing of the photodiode amplifier outputs and to also complete the intensity dependence study described below.

The Iodine cells themselves are contained in a glass tube oven constructed from a larger diameter pyrex testube. In our implementation the tube oven was large enough to accomo-

date a heater, a K-type thermocouple and two depleted Iodine cells. For compactness, the heater was made with about 35cm of nichrome wire (total resistance $\sim$ 1 Ohm) threaded first through a 11cm long thin glass tube and then wound around the outside of that tube in a helix. The entire tube oven was (except for the needed optical access) surrounded by thermal wool and supported horizontally on a chem-stand. A small wadding of thermal wool inside the head and back (open end) of the tube oven served to further thermally isolate the vapor cells to arrive quickly at 480^oK using less than 12 Watts of heat, as the heater was driven by a PWM switched NTP5411NG mosfet connected to a 12V DC supply.

Any fixed temperature difference between the thermocouple and the cell does not enter into the error budget for our measurement since such an overall offset does not alter the slope. However, if there is a difference, then there will be a spatial gradient between the cell and the thermocouple whose magnitude gets progressively smaller during cool down in proportion to the temperature difference between the inside and outside of the tube oven. We have not endeavored to measure this difference OR correct for it in the data described here, being instead careful to minimize it by co-locating the thermocouple and cell.

The laser diode's current was driven by a commercial laser diode driver (Thorlabs TCM1000T or equivalent) and the diode itself was mounted in a thermal block (aluminum) with small resistive heaters and a thermistor, surrounded by a styrofoam package with a glass aperture for the laser beam (to reduce air infiltration). The thermistor and heaters were connected to a Arduino UNO running a basic PID code (in a configuration identical to and running the same code as that described in detail in[24]). In practice this lead to laser optical frequency drifts of less than a few MHz per minute which further simplified the analysis of each data set, collected typically over the span of 30 minutes.

Before describing the experimental protocol further we mention that we felt it necessary to also calibrate the Fabry-Perot (FP) cavity used throughout as a frequency ruler. The traditional way to calibrate this is against a optical reference, and here using the Iodine atlas to identify pairs of resonances with a known frequency interval would have been useful. Another way to calibrate the FP is to use an electro-optic modulator (EOM) or acousto-optical modulator (AOM) to create sidebands some 100's of MHz apart and record their positions relative to the dominant FSR-spaced lines in the Fabry-Perot output. Note that for the diodes we used it was not practical to modulate them directly (via current modulation) at a sufficiently high frequency, so use of an external EOM/AOM would have been unavoidable.

TABLE I. Typical costs associated with this laboratory, excluding basic laboratory glass tubing and basic electrical connectors, thermocouples, meters, laboratory power supplies and digitizing 200MHz oscilloscope and computer.

Name	cost	comment/vendor
Laser Diode	\$16	Mouser Electronics
Iodine	\$30	Flinn Scientific
FP cavity	\$3627	Thorlabs SA200-5B
Asst. Optics	\$1700	Thorlabs 3 VND, 1 waveplate
Asst. Electronic	\$28	Cost for 2 ea. of TL062 and BPW 34 S, Arduino Uno, mosfet
Current controller	\$455	Thorlabs TCM1000T
Total	**\$ 5856**	

The simplest calibration option for our laboratory was to reference its resonances against the Saturated Absorption (SAS) features of Rubidium at 780nm. This results in sub-doppler features (Fig. 3), including prominent cross-over features due to the F=2→ F'=2,3 and the F=1→ F'=1,2 transitions in 87Rb. We use the known frequency interval between those features (=6.623 GHz) to determine the Free Spectral Range (FSR) of our FP to be 1510 ± 15 MHz. Since the FP is an air-filled confocal type we expect that this is, within errors, the same FSR at 520nm.

In our implementation of this experiment, we align the cylindrical cell to be interrogated so that the signal beam goes through its middle. Of course this distorts the exciting beam but by placing our sensor behind an aperture but within a few centimeters of the cell we can easily identify absorption resonances even at room temperature at good contrast ($\sim$ 10%). While a temperature control loop for the diode is used for coarse frequency tuning, the diode current controller's modulation input is connected to a low frequency (10 Hz) triangle wave generator for finer frequency adjustment. In this way the current, and thus, the laser's optical frequency is ramped mode-hop free over typically a few GHz. With the Fabry-Perot cavity alinged with part of the reference beam to give deep ($\sim$.2V), symmetrical resonances, we align the rest of the reference beam on its photodiode and then balance the two detectors

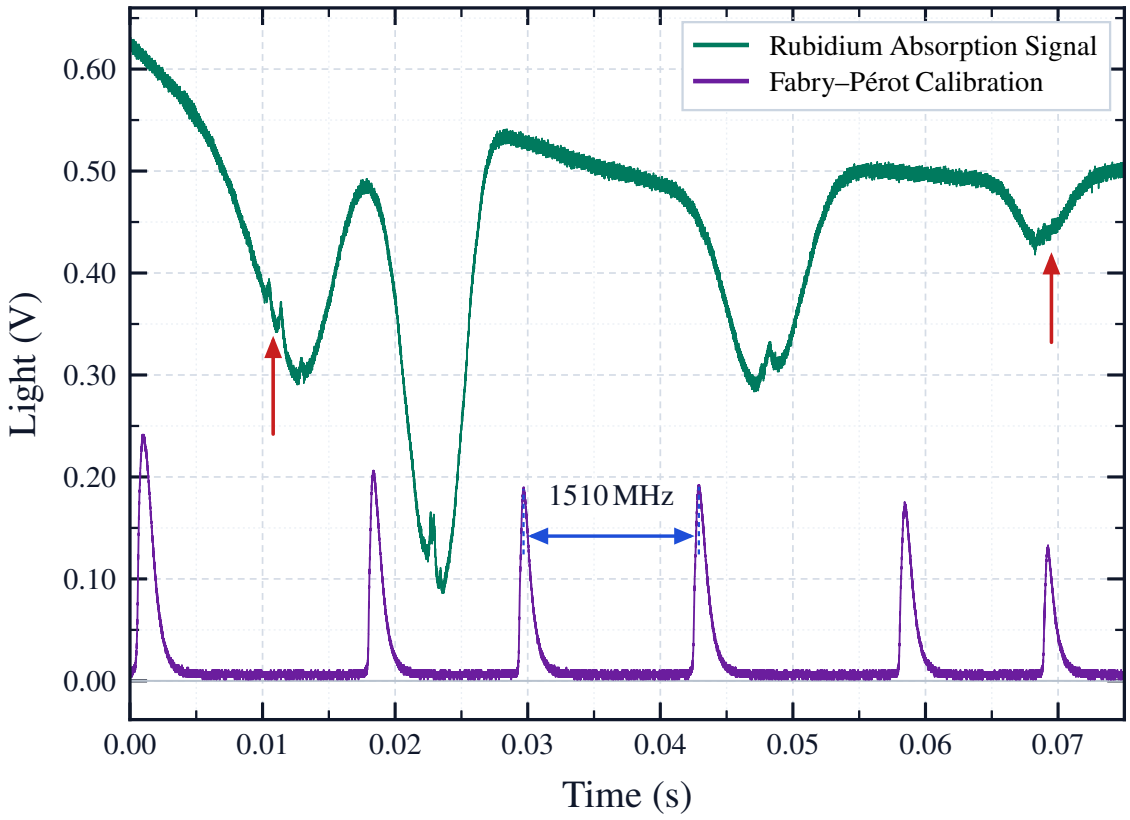

FIG. 3. Calibration of the Fabry-Perot (FP) cavity at 780nm using (natural abundance) Rubidium vacuum vapor cell SAS at room temperature (uppermost trace, green). The FP cavity FSR is then 6.623 GHz divided by the total number of FP resonances (lower trace, purple) by linear interpolation between the two large SAS cross-over features in the ^{87}Rb, here indicated with red arrows.

using variable neutral density filters, displaying the amplified difference on the oscilliscope. One of the variable neutral density filters is before the reference photodiode and the other two are placed before and after the Iodine cell. This last pair simplifies our study of the power dependence of the linewidth, for extrapolating a broadening measurement to zero power. Note that since polarization plays no role in this experiment, and since the laser light is strongly polarized, a single or pairs of linear polarizer sheet may be used instead of variable neutral density plates.

Once we tune the laser to locate a reasonable contrast, isolated and symmetrical absorption feature at room temperature, we turn on the heating of the tube oven. After it reaches 480°K we turn off the heating and record the absorption line each 10 degrees decrease as

it cools back down to room temperature over the span of 30 minutes. For fitting purposes it is important that each trace has about as much time on and off the absorption feature; that is, the "wings" of the feature need to occupy nearly as much of the trace as the central resonance as in Fig.4. An accurate accounting of the resonance width is dependent on the wings, and in a undepleted cell the growth of the optical depth also causes off-resonant darkening in the "wings" that, when fit with a simple Gaussian, can obscure the Doppler growth of the width.

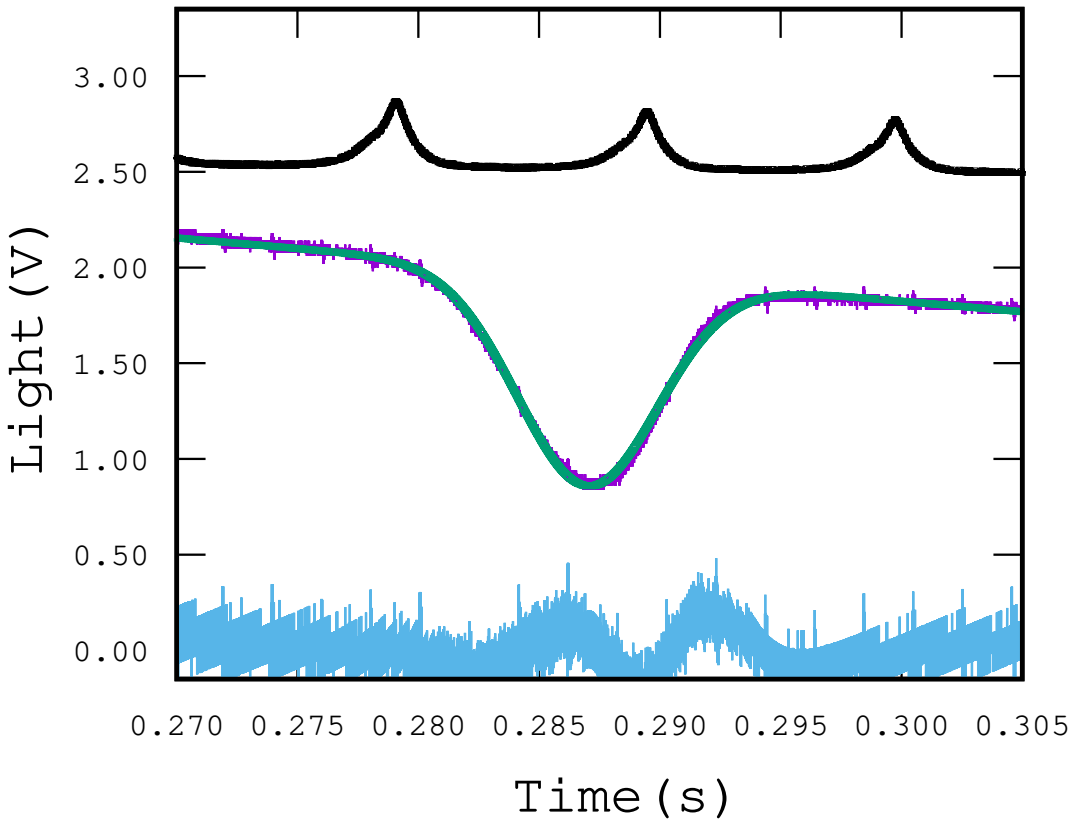

FIG. 4. Typical Oscilloscope trace of balanced detection data (middle trace, purple) co-plotted with its Gaussian best fit (green) of an iodine resonance in a narrow, depleted cell at 410°K. Shown also (lower trace, in blue) are the fit residuals magnified by a factor of 5. Also shown (top trace) are the simultaneously recorded Fabry-Perot cavity transmission resonances, offset vertically for clarity.

III. ANALYSIS AND DISCUSSION

Each absorption feature's traces at temperatures between 310^oK and about 480^oK are digitized and fit with a single Gaussian using the Marquardt-Levenberg routine in MATLAB™, or Octave or Gnuplot. We have done this for many different Iodine absorption features (results for about 12 shown below). In practice it is also necessary to include an offset a and a slope b in the fit, as

$$y(t) = a + b(t - t_0) + ce^{-\frac{(t-t_0)^2}{2w^2}} \tag{4}$$

This significant simplification over more complex fitting schemes such as multi resonant fitting and Voigt function fitting is possible since the vapor cell is optically (since it is depleted) and physically thin throughout the entire experiment. As pointed out earlier, at a pedagogic level this greatly assists students making the connection between the Doppler effect, the Maxwell distribution with the fact that during the trace, as a consequence of the triangular wave modulation, the frequency change of the laser is nearly proportional to the time 't'. Fitting these data with Eq.4 is also very quick and in less than 20 minutes students can assemble a summary chart of the fit parameters at each temperature.

To that chart the conversion factor from temporal intervals to frequency interval is accomplished by recording time between adjacent Fabry-Perot resonance maxima on either side of the resonance, and equating that time to the FP cavity's calibrated FSR as describe earlier. In practice we find that non-linearities in the temporal advance of the frequency between Fabry-Perot resonances are far too small to contribute appreciably to the error budget for the resonance width. Typically during the duration of the experiment the time difference between the relevant adjacent Fabry-Perot resonances varies by less than 0.2%.

Finally then a graph of the measured (full Gaussian-)width-squared versus temperature is fit with a straight line, as in Fig.5a. As described above, the slope of that line is the square of the overall temperature coefficient of the width which chiefly includes a Doppler coefficient $k_B/m\lambda^2$ and a collisional term proportional to the square of the number density (which is basically independent of temperature over a range in these cells). For the data in Fig.5a, we find a line slope of 478 ± 55 $\text{MHz}^2/^o\text{K}$, leading to an overall temperature coefficient of (21.9 ± 1.5) $\sqrt{(}T)$ MHz, quite close to the expected 22.05 $\sqrt{(}T)$ MHz value for the Doppler coefficient for molecular Iodine.

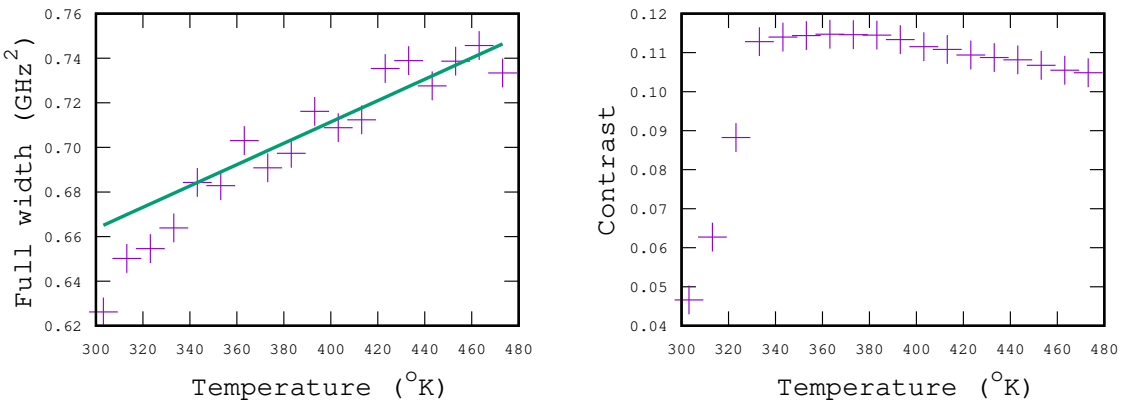

FIG. 5. (a) Plot of the square of the resonance width of an absorption feature in a depleted cell with temperature. The linear fit shown uses only data above 330°K, as the absorption line contrast (shown in (b)) is less variable there. Optical power incident on the cell was 25 μW, and the beam diameter was about 1mm, corresponding to an estimated intensity of 3 mW/cm^2

Potentially complicating atributing this measurement to the Doppler contribution would be any temperature-dependent optical power effect on the resonance shape and width. It is worth noting that in isolated resonances and systems without degeneracies, increasing the power generally causes power broadening. One way to think of that effect is via the uncertainty principle. The intrisic spectral width of an isolated fluorescent state is inversely proportional to its lifetime, the ground state having no flourescence thus has no intrinsic spectral width. When the atom/molecule is illuminated the absorption process from the ground state to the excited state means that the ground state effectively becomes unstable to decay to the excited state. Similarly the excited state's lifetime is also reduced due to stimulated emission. Both effects, since they reduce the residency time in either state, contribute positively to the growth of the measured spectral width of the transition.

However in more complex level schemes, typically in which there are multiple transitions contributing under a single Boltzmann envelope that correspond to distinct nearly degenerate ground state, the opposite effect occurs, called power narrowing. One way this can happen is that as one first enters the Doppler envelope the underlying states are subject to differential excitation rates. This tends to organize the ground state atoms and molecules into dark states, effectively reducing the absorption in the wings of the Doppler envelope which may then be recorded as a reduction in the Doppler broadening.

These relaxation processes that control the degree to which molecular populations are "sculpted" by optical processes are themselves temperature dependent, leading to a contribution to the observed temperature dependence of the resonance width. To avoid these temperature-dependent optical power contributions it is important to operate the entire experiment well below the resonance's saturation threshold. Although these power-dependent effects are not expected to be strictly linear, for simplicity one can partially address this dependence by measuring the temperature dependence of the width of the same resonance at a few different powers and extrapolating linearly to zero power. We note that we have quantified both power narrowing and power broadening on different molecular Iodine transitions and its effect on the retrieval of the universal Doppler contribution to the width, but below report primarily the results of this protocol at low optical power where the effect is expected to contribute less than the reported errors of our measurement.

Finally, we address empirically how well these methods suffice to isolate the universal Doppler coefficient by doing the analysis on a series of different transitions and with different 520nm laser diode sources as shown in Figure 6. There is plotted the square root of each slope of the (width)^2 versus temperature graph from our Gaussian fits. The data shown is of three different 520nm lasers interrogating 12 different molecular Iodine transitions. All the data shown is for thin (millimeters thick) vacuum vapor cells made by the student co-authors. The first point (cross) is from an undepleted cell as in Fig. 1. The "x"s that follow that are a few different resonances probed with a constant vapor pressure vacuum Iodine cell, as in Ref.[19] While both of these approaches may give reasonable estimates of the slope expected from theory (red line) they tend to have large fit errors due to covariance associated with large contrast changes.

The rest of the data show in Fig. 6 were taken using thin, depleted vacuum Iodine cells made as described earlier in the methods section of the paper. Because of covariances between fit moduli it important to select for study resonant features that are as symmetrical and isolated as possible. For example, data shown as blue stars were purposefuly taken from two different absorption features that were, by eye, clearly not symmetric. To perform the fit on these data we used two Gaussians, reporting in the figure the dominant width's changes with temperature. The fit covariances associated with large asymmetry lead to uniformly smaller temperature growth of the width.

As remarked, optical power must also be kept below any pumping or line broadening

threshold. Each pair of tan open boxes and solid yellow squares are two different symmetric, isolated absorption feature, but with the optical power entering the vapor cell being 6 times higher for the tan open box data than the solid yellow squares (the later intensity being about 1.5 mW/cm^2). Note that this is not an artifact associated with the detector sensitivity, as we adjusted the for- and aft-cell VNDs to have nearly the same amount of light on the PD each run. We also have data from other absorption features in which the higher optical power leads to Doppler slope estimates above both the theoretical value and the lower power slope (not shown in figure) for that absorption feature. While the variances are about the same, for better accuracy we recommend performing this width measurement at or below an intensity of 3 mW/cm^2 in this 520nm range.

Finally, the solid yellow squares and the open blue circles are from other spectrally isolated, symmetric absorption features in multiple depleted, thin cells, at low optical power. We simply note that these data typically have significantly smaller variances than the data from either the constant pressure or undepleted thin cells, while also clustering around the value expected from simple kinetic theory.

IV. CONCLUSION

Going forward we are addressing some of the systematics affecting the overall accuracy of the measurement. For example, one simple possible improvement would be to improve the thermometry of the cell within the tube oven, or otherwise redesigning the oven to minimize the internal thermal gradients. Even without changing anything inside the tube oven itself, simply insulating it better and slowing down its approach to equilibrium would help in this regard, even still while keeping its entire duration well within a laboratory class period.

We have also attempted to compare two differently loaded depleted cells on the same absorption feature. Since the maximum Iodine pressure would be different in each this may allow us to quantify any residual resonant scattering effect. Looking at the temperature at which the contrast curves saturate in each cell using the Antoine equation may give a crude estimate of the relative number density of Iodine in these cells, as would perhaps directly comparing the depth of the same absorption features in each cell. While this may provide additional insights into the systematics and the spread of Doppler slope values we find across different transitions, it remains a future direction that is beyond this laboratory's current

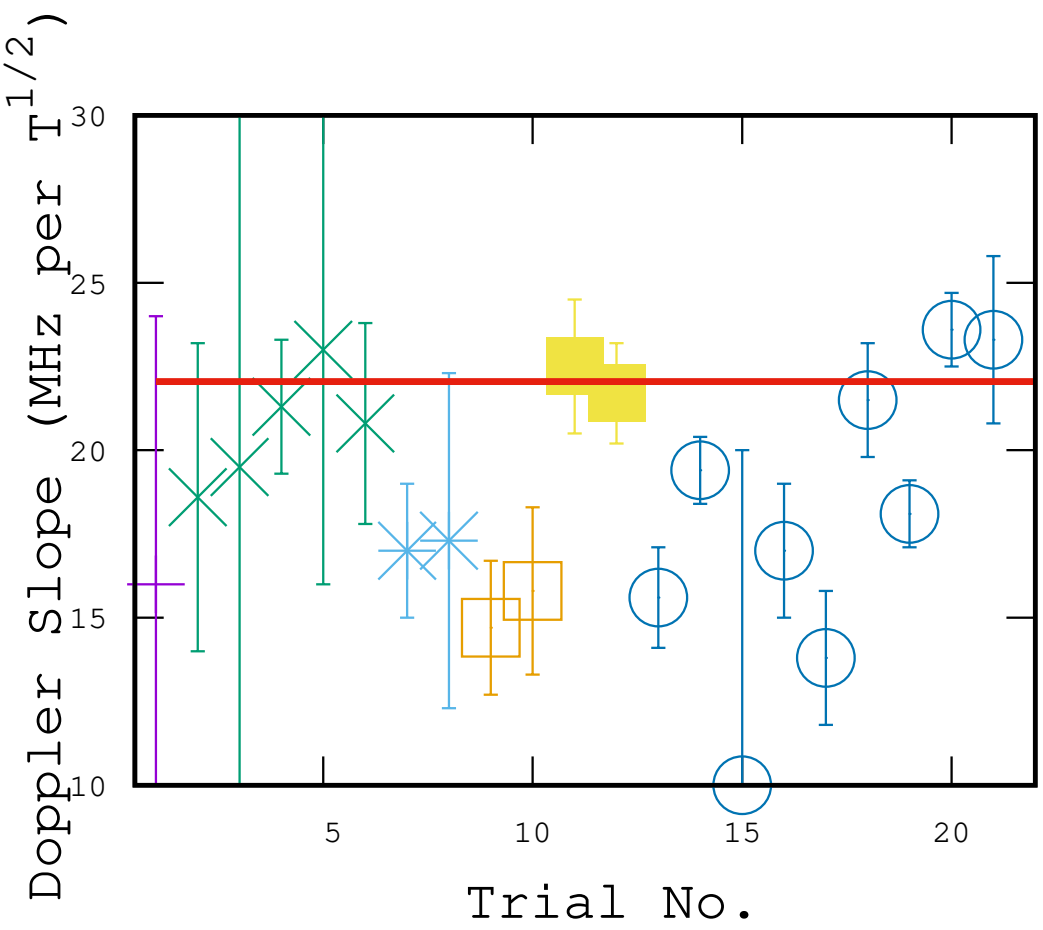

FIG. 6. (a) Plot of the measured Doppler slopes of distinct molecular iodine transitions near 520nm as measured all in narrow student-made vacuum cells. The (purple) cross is typical data from an undepleted cell. There the dramatic line contrast changes tend to lead to large fit errors. The constant pressure cell data collected at different transitions had a somewhat similar systematic (green "X"s) and large variances. In the depleted cells even at low optical power (two different) grossly asymmetric absorption lines that had to be fitted with two gaussians resulted uniformly in values of the Doppler slope below the theoretical value (blue stars). All of the other data shown is from isolated rather symmetrical absorption features. Operating at large optical intensities (well above $\sim$ 10 mW/cm^2) tended to lead to large systematic effects (tan open squares) as well. The yellow squares are from data collected at the same transitions as the two tan open squares, but at much lower intensities ($\sim$ 1.5 mW/cm^2). Data from isolated, rather symmetrical absorption lines in depleted cells at low power (yellow squares and blue circles) tended to have lower errors and cluster somewhat around the theoretical value (red line).

compact protocol.

By freezing bromine then loading and evacuating the cells while cold we have also created depleted molecular Bromine cells. Due to its lower molecular mass the Doppler slope is expected to be larger for Bromine. However the optically accessible absorption features in molecular Bromine that we have surveyed around 520nm appear to be spectrally somewhat broad, as in so-called "molecular band heads," making them unsuitable for this protocol. Using lasers in the 560nm range may simplify the spectrum enough to allow for analysis in the protocol here.

Although going to higher temperature with vacuum molecular Iodine one might think would lead to better data for this study, there is an important limitation. As one increases the temperature much above 500^oK, although the cell doesn't continuously darken off resonance as in the undepleted cells, the line contrast will quickly evolve ever lower with temperature as the so-called "hot branch" (*i.e.* states connected to the ground vibrational states) emerges in the absorption spectrum. Since changes in the feature contrast tend to lead to larger errors in width change due to a fit covariance any gain from accessing higher temperatures will be, at best, muted.

In conclusion, the dearth of undergraduate laboratory experiences which directly measure the (optical) Doppler effect in spectroscopy stems from the fact the effect is ordinarily obscured by a plethora of interesting but extraneous physical processes. By using thin depleted (*i.e.* sometimes called vapor-limited) vacuum (molecular) Iodine cells and readily available low-power laser diodes near 520nm we have shown that with Gaussian fitting alone students can achieve measurements of the Doppler effect that is within 15% of the value expected by kinetic theory.

In addition to displaying a universal wave phenomenon at play for light in moving absorbers and its connection to kinetic theory and statistical mechanics, this laboratory reinforces familiarity with basic optical metrology, including the use of Fabry-Perot cavity resonances and balanced photodetection.

ACKNOWLEDGMENTS

This work was supported in part by the U.S. National Science Foundation (Grant NSF-DMR-2226956), and the Williamson Watanakunakorn Summer Science Program and the Ann Seimon Endowment administered through Youngstown State University.

V. AUTHOR CONTRIBUTIONS

SC, VTC, DM , NH, EH, CV were primarily involved in experimental development, modification and data collection, TA and MD were tasked mostly with analysis and manuscript preparation, RS and MD were primarily involved in theory sections and its numerical evaluation, and MC was involved in the experiment setup, data analysis, theory sections and manuscript preparation.

VI. AUTHOR DECLARATION

The authors have no conflicts to disclose.

---

* cadenvernon@gmail.com, mdahal03@student.ysu.edu, dgminich@student.ysu.edu, eliemanuel2008@gmail.com, Nathanjh908@gmail.com, teayers@student.ysu.edu, sccart@student.ysu.edu, vtobarcorrea@student.ysu.edu, restipanovich@student.ysu.edu, dcphtn@gmail.com

[1] E. L. Lewis, "Collisional Relaxation of Atomic Excited States, Line Broadening and Interatomic Interactions," Phys. Rep. **5**8,#1, 1–71 (1980).

[2] C. Daussy, M. Guinet, A. Amy-Klein, K. Djerroud, Y. Hermier, S. Briaudeau, Ch. J. Bordé, and C. Chardonnet, "Direct Determination of the Boltzmann Constant by an Optical Method," Phys. Rev. Lett. **9**8, 250801 (2007).

[3] G. Casa, A. Castrillo, G. Galzerano, R. Wehr, A. Merlone, D. Di Serafino, P. Laporta and L. Gianfrani, "Primary Gas Thermometry by Means of Laser-Absorption Spectroscopy: Determination of the Boltzmann Constant," Phys. Rev. Lett. **1**00, 200801 (2008).

[4] L. Gianfrani, "Linking the thermodynamic temperature to an optical frequency: recent advances in Doppler broadening thermometry," Phil. Trans. R. Soc. A **3**74 20150047 (2016).

[5] G. T. Phillips, G. P. Perram, "Pressure broadening by argon in the hyperfine resolved P(10) and P(70) (17,1) transitions of I2 using sub-Doppler laser saturation spectroscopy," Journal of Quantitative Spectroscopy & Radiative Transfer, **1**09, 1875–1885 (2008).

[6] A. Nishiyama, S. Okubo, T. Kobayashi, A. Kawwasaki, and H. Inaba, "Measurement of transition frequencies and hyperfine constants of molecular iodine at 520.2 nm," Journal of the Optical Society of America B, **41**, # 10, pp. 2290-2296 (2024).

[7] Y-H. Chen, W-C. Lin, J-T Shy and H-C. Chui, "Iodine-stabilized single-frequency green InGaN diode laser," Optics Letters, **43** #1, 126–129 (2018).

[8] L.Yu, L. Cao, Z. Yue, L. Li, and Y. Zhai, "In situ temperature measurement of vapor based on atomic speed selection," Chin. Phys. B **32**, 020602 (2023).

[9] S. M. Bresler, E. M. Adkins, S. P. Eckel, T. K. Herman, D. A. long, B. J. Reschovsky and D. Barker, "Electro-optic frequency comb Doppler-broadening thermometry," Optics Express, **34**, #7 12121–12131 (2026).

[10] N. Agnew, V. Vohnikova, E. Riis, G. Machin, and A. S. Arnold, "Practical primary thermometry via alkali-metal-vapour Doppler broadening," Phil. Trans. R. Soc. A **384** 20240455 (2026).

[11] G. W. Truong, E. F. May, T. M. Stace, A. N. Luiten, "Quantitative atomic spectroscopy for primary thermometry," Phys. Rev. A **83**, 033805 (2011).

[12] G.-W. Truong, J.D. Anstie, E.F. May, T.M. Stace and A.N. Luiten, "Accurate lineshape spectroscopy and the Boltzmann constant," Nat. Comms. **6** #8345 (2015).

[13] G-W. Truong, D. Stuart, J. D. Anstie, E. F. May, T. M. Stace and A. N. Luiten, "Atomic spectroscopy for primary thermometry," Metrologia **52** S324–S342 (2015).

[14] S Wójtewicz , P Wcislo , P Amodio , L Gianfrani , D Lisak and R Ciurylo, "Dispersion and relativistic corrections to the spectral line-shape models," IOP Conf. Series: Journal of Physics: Conf. Series **810** 012062 (2017).

[15] Y. Pan, W. Liao, H. Wang, Y. Yao, J. Cai and J. Qu, "Cesium atomic Doppler broadening thermometry for room temperature measurement," Chin. Opt. Lett. **17**, #6, 060201 (2019).

[16] R. Gotti, M. Lamperti, D. Gatti, and M. Marangoni, "Laser-Based Primary Thermometry: A Review," J. Phys. Chem. Ref. Data **50**, 031501 (2021).

[17] D Pizzey, J. D. Briscoe, F. D. Logue, Francisco Sebastian Ponciano Ojeda, S. A. Wrathmall, I. G. Hughes, "Laser spectroscopy of hot atomic vapours: from 'scope to theoretical fit," New Journal of Physics, **24**, pp.125001 (2022).

[18] N. M. Lawandy, "Temperature Dependence of Optically Pumped Far-Infrared (FIR) laser output power," Infrared Physics, **19** #19 127-134 (1979).

[19] C. Leahy. J. T. Hastings, P. M. Wilt, "Temperature dependence of Doppler-broadening in rubidium: An undergraduate experiment" American Journal of Physics **6**5, 367 (1997).

[20] T Vartanyan, V Polishchuk, A Sargsyan, A Krasteva, St Cartaleva and G Todorov, "Temperature and excitation power influence on the velocity-selective optical pumping resonances of 133Cs atoms confined in an extremely thin cell", J. Phys.: Conf. Ser. **9**92 012023 (2018).

[21] Z. Zhang, W. You, X. Liu, H. Liu, W. Yuan, J. Zhang, K. Deng and Z. Lu, "High performance molecular iodine optical reference using an unsaturated vapor cell," Rev. Sci. Instrum. **9**5, 063003 (2024).

[22] NIST Chemistry WebBook, SRD 69, (2026), https://webbook.nist.gov/cgi/cbook.cgi?ID=C7553562&Mask=4&

[23] S. Gerstenkorn and P. Luc, Atlas Du Spectre D'Absorption De La Molécule D'Iode, 14800-20000 cm^{-1} (Centre national de la recherche scientifique, 1978).

[24] A. Anderson, T. Ayers, B. E. Bish, S. Cart, V. Tobar Correa, A. O'Brien, R. Stipanovich and M. Crescimanno, "Rubidium isotope shift measurement made simple," Amer. J. Phys., **9**4, 575–581 (2026).

[25] L. Boltzmann, "Weitere Studien über das Wärmegleichgewicht unter Gasmolekülen," *Sitzungsberichte der Akademie der Wissenschaften*, **66**, 275–370 (1872).

[26] L. Boltzmann, "Further Studies on the Thermal Equilibrium of Gas Molecules," in *The History of Modern Physical Sciences*, **1**, 262–349 (2003), doi:10.1142/9781848161337_0015.

[27] J. C. Maxwell, "Illustrations of the Dynamical Theory of Gases.–Part I. On the Motions and Collisions of Perfectly Elastic Spheres," *The London, Edinburgh, and Dublin Philosophical Magazine and Journal of Science*, **19**, 19–32 (1860), doi:10.1080/14786446008642818.

[28] J. C. Maxwell, "On the Dynamical Theory of Gases," *Philosophical Transactions of the Royal Society of London*, **157**, 49–88 (1867), doi:10.1098/rstl.1867.0004.

VII. SUPPLEMENTARY MATERIAL

For completeness, we briefly review the basics of kinetic theory as formulated by Maxwell before the advent of the Boltzmann-Gibbs formulation of statistical mechanics. Since the latter is typically more familiar to students, we adopt the notation $< \mathcal{O} >= \int f(a)\mathcal{O}(a)da$ and $f(a)$ is some normalized distribution $\int f(a)da = 1$ defining the equilibrium state of the

gas at temperature T and total number density n. In equilibrium we expect then $< v_i >= 0$ but $< v_i^2 > \neq 0$ where $i = x, y$ or z. Then Maxwell kinetic theory for the pressure assuming specular reflection yields,

$$P = (collisionrate/area) \cdot (2mv_x) = (\frac{n}{2}v_x)2mv_x = 2nm < v_x^2 > \tag{5}$$

Using now the ideal gas law $PV = Nk_BT$, $(n = N/V)$ indicates that $\frac{m}{2} < v_x^2 >= \frac{1}{2}k_BT$, a familiar equipartition theorem result that preceeded Maxwell's approach to Eq. 5 by 13 years. Note the full specification "ideal gas" refers to both the ideal gas law combined with a formula for the total internal energy, which by isotropy for the above identification $U = \frac{Nm}{2} < v_x^2 + v_y^2 + v_z^2 >= \frac{3}{2}PV$.

Students are generally most familiar with the direct derivation of the Maxwell-Boltzmann distribution using the Boltzmann factor from the canonical ensemble. However, Maxwell originally derived the equilibrium velocity distribution in 1860, twelve years prior to Boltzmann's 1872 kinetic argument[25–27]. In his 1860 paper, Maxwell assumed that the probability distribution of one Cartesian velocity component was independent of the knowledge of another component. He later described this assumption as "precarious" and, in his 1867 paper, replaced it with a more physically justified collision-based argument[28]. We sketch below in contemporary terms Maxwell's later argument as imposing stationarity of the equilibrium velocity distribution together with microscopic reversibility of molecular encounters. This results in detailed balance between forward and reverse collision processes.

For the mathematical formulation of Maxwell's 1867 argument, first consider a large ensemble of particles undergoing binary elastic collisions within an isotropic gas. Maxwell assumed three principal conditions: (a) at equilibrium, the number of particle pairs whose velocities change from $(\vec{v}_1, \vec{v}_2) \to (\vec{v}_3, \vec{v}_4)$ equals the number undergoing the reverse transition, from $(\vec{v}_3, \vec{v}_4) \to (\vec{v}_1, \vec{v}_2)$, which we refer to as the condition of detailed balance; (b) repeated molecular encounters rapidly establish an equilibrium velocity distribution $f(\vec{v})$ that remains stationary, i.e., time-independent; and (c) the underlying elastic two-body collision process is microscopically reversible, so the physical process is time-reversal symmetric.[28] To express these conditions in contemporary kinetic-theory notation, let $W(1, 2; 3, 4)$ denote the scattering kernel for the binary process

$$1 + 2 \to 3 + 4$$

Here, $1, 2, 3, 4$ denote the respective single-particle momentum or velocity states. In the modern Boltzmann collision-integral framework, the collision process described above is expressed as

$$\left(\frac{\partial f(1,2)}{\partial t}\right)_{\text{col}} = \int\int \left[W(3,4;1,2)f(3)f(4) - W(1,2;3,4)f(1)f(2)\right] d^3p_3 d^3p_4 \tag{6}$$

Since the distribution is stationary, $\left(\frac{\partial f(1,2)}{\partial t}\right)_{\text{col}} = 0$, so (6) is set equal to zero.

$$0 = \int\int \left[W(3,4;1,2)f(3)f(4) - W(1,2;3,4)f(1)f(2)\right] d^3p_3 d^3p_4 \tag{7}$$

Detailed balance stipulates that the rate of each individual scattering process equals the rate of its reverse process. Consequently, the bracketed term in (7) is zero.

$$W(3,4;1,2)f(3)f(4) - W(1,2;3,4)f(1)f(2) = 0 \tag{8}$$

This result implies $W(3,4;1,2)f(3)f(4) = W(1,2;3,4)f(1)f(2)$. Time-reversal symmetry of the collision process further requires that the kernel $W(1,2;3,4) = W(3,4;1,2)$, so (8) reduces to

$$f(3)f(4) = f(1)f(2) \tag{9}$$

Taking the natural logarithm of both sides and applying elementary logarithmic identities, (9) reduces to

$$\Phi(1) + \Phi(2) = \Phi(3) + \Phi(4) \tag{10}$$

where $\Phi(i) = \ln\left(f(i)\right)$, with $i \in \{1, 2, 3, 4\}$. Since the system under consideration consists of elastic collisions, three quantities are conserved:

- $\vec{p}_1 + \vec{p}_2 = \vec{p}_3 + \vec{p}_4$ (momentum conservation)
- $E_1 + E_2 = E_3 + E_4$ (Energy conservation)
- Particle number

Therefore, we expect

$$\Phi(i) = \alpha + \vec{\beta} \cdot \vec{p}_i + \gamma E_i \tag{11}$$

Here, $\vec{p}_i$ and E_i denote the momentum and energy of the ith particle, α and γ are scalar constants and $\vec{\beta}$ is a vector constant. Assuming there is no bulk motion of the gas, isotropy reduces to $\vec{\beta} = 0$, so (11) reduces to

$$\Phi(i) = \alpha + \gamma E_i \tag{12}$$

From which we learn $f(E_i) = Ae^{\gamma E_i}$. Finally, being bounded in $E_i > 0$ then implies $\gamma < 0$ and the kinetic theory deliberations (namely, equipartition) identify the second moment of the distribution with $k_B T$ fixing $\gamma = -\frac{1}{k_B T}$ uniquely. Note that this argument makes no assumptions about the masses of the gas atoms/molecules all being the same. Note however that for identical bosons (respectively fermions) Maxwell's same three considerations lead to

$$f(1)f(2)(1 \pm f(3))(1 \pm f(4)) = f(3)f(4)(1 \pm f(1))(1 \pm f(2)) \tag{13}$$

where the extra factors come from (upper sign) Bose stimulated emission (respectively Pauli blocking, lower sign) in the final state of each scattering process. When one then cross multiplies this expression isolating the '1' and '2' - dependent term on one side and the '3' and '4' on the other, the same considerations as in the classical case above lead to the Bose-Einstein (respectively the Fermi-Dirac) distributions. In this approach terms proportional to the change in the entropy of system under the scattering appear on both sides. In this view then, Eq.9 and Eq.13 expresses the extremality of the total entropy under collision processes, resulting in stationary equilibrium distributions.

VIII. DATA AVAILABILITY

All the data taken during this experiment is available upon request to the authors.